Nanoscale Res Lett (2008) 3:372–380
DOI 10.1007/s11671-008-9169-6

NANO EXPRESS

Optimization, Yield Studies and Morphology of WO_3 Nano-Wires Synthesized by Laser Pyrolysis in C_2H_2 and O_2 Ambients—Validation of a New Growth Mechanism

B. W. Mwakikunga · A. Forbes · E. Sideras-Haddad · C. Arendse

Received: 28 July 2008 / Accepted: 3 September 2008 / Published online: 25 September 2008

Abstract Laser pyrolysis has been used to synthesize WO_3 nanostructures. Spherical nano-particles were obtained when acetylene was used to carry the precursor droplet, whereas thin films were obtained at high flow-rates of oxygen carrier gas. In both environments WO_3 nano-wires appear only after thermal annealing of the as-deposited powders and films. Samples produced under oxygen carrier gas in the laser pyrolysis system gave a higher yield of WO_3 nano-wires after annealing than the samples which were run under acetylene carrier gas. Alongside the targeted nano-wires, the acetylene-ran samples showed trace amounts of multi-walled carbon nano-tubes; such carbon nano-tubes are not seen in the oxygen-processed WO_3 nano-wires. The solid–vapour–solid (SVS) mechanism [B. Mwakikunga et al., J. Nanosci. Nanotechnol., 2008] was found to be the possible mechanism that explains the manner of growth of the nano-wires. This model, based on the theory from basic statistical mechanics has herein been validated by length-diameter data for the produced WO_3 nano-wires.

Keywords Laser pyrolysis · Tungsten trioxide · Nano-wires · Growth mechanism

B. W. Mwakikunga (✉) · C. Arendse
CSIR, National Centre for Nano-Structured Materials, P.O. Box 395, Pretoria 0001, South Africa
e-mail: bmwakikunga@csir.co.za

B. W. Mwakikunga · E. Sideras-Haddad
School of Physics, University of the Witwatersrand, Private Bag 3, P.O. Wits 2050 Johannesburg, South Africa

B. W. Mwakikunga
Department of Physics and Biochemical Sciences, University of Malawi, The Polytechnic, Chichiri, Private Bag 303, Blantyre 0003, Malawi

A. Forbes (✉)
CSIR National Laser Centre, P.O. Box 395, Pretoria 0001, South Africa
e-mail: aforbes1@csir.co.za

A. Forbes
School of Physics, University of Kwazulu-Natal, Private Bag X54001, Durban 4000, South Africa

Introduction

Amongst many transition metal oxides, WO_3 has excellent electro-chromic, gaso-chromatic and photo-chromatic properties. At room temperature it adopts the distorted monoclinic structure of ReO_3 [1]. For this reason, WO_3 has been used to construct flat panel displays, photo–electro–chromic 'smart' windows [2–4], writing–reading–erasing optical devices [5, 6], optical modulation devices [7, 8], gas sensors and humidity and temperature sensors [9–11]. Self assembly of these materials has been achieved by hydro-thermal techniques, additive-free hydrothermal means, templating either with a polymer or pre-assembled carbon nano-tubes, epitaxial growth, sol-gel, electro-chemical means and hot-wire CVD methods. Recently, WO_3 nano-rods produced by a facile chemical route and CVD have been reported [12, 13] in this journal. In laser pyrolysis, authors have reported synthesis of, for instance, ceramics, silicon and silicon compounds, carbon compounds, olefins, chromium oxides, diamond, fullerenes and many other classes of materials. These experiments have largely been performed at high laser powers and hence at high temperatures. At such high levels, where anharmonicity cannot be ruled out, laser pyrolysis is equivalent to traditional pyrolysis with the photo-thermal process overwhelming the

photo-chemical one. However, it has long been realized that even at low intensity, the CO_2 laser has successfully been used in the synthesis of boron compounds from BCl_3 [14, 15]. At these low power values, the laser is used to selectively excite the reactant to a relatively low vibrational level from which a chemical reaction with other reactants present is initiated. One expects to achieve product formation distinctly different from that achieved by traditional pyrolysis for the same chemical reaction provided that the laser energy absorbed is channelled mainly into the chemical process rather than into heating.

In this Letter, we report optimization of parameters that led to the synthesis of WO_3 nano-spheres and thin films at relatively low laser power (50 W in a 2.4-mm focal region). We demonstrate the role of thermal annealing in the conversion of the spheres and slabs into nano-wires. We also show the morphological differences and yields when carrier gases—C_2H_2 or O_2—are used during the synthesis.

Experimental

Our laser pyrolysis experimental set up was fully described in our previous publication [16]. Briefly, the method involves injecting a stream of very fine droplets of a precursor solution into an infrared laser beam and depositing the resulting aerosol onto a Corning glass substrate. A wavelength tuneable continuous wave (cw) CO_2 laser was used in the experiments (Edinburgh Instruments, model PL6). By selecting a wavelength of 10.6 μm, the laser was within, but not exactly on, the absorption region of the pre-made precursor (WCl_6 in ethanol or tungsten ethoxide) for the production of WO_3. From the fact that (1) the excitation wavelength of 10.6 μm is not exactly at the main resonance peak of the W-ethoxide precursor of 9.44 μm and (2) the laser power of 50 W (focussed into 2.4-mm beam diameter at the waist) is not low enough to rule out anharmonic effects in the excitation, the decomposition of this precursor could be due to both photochemical (resonance) and photo-thermal (anharmonic) processes. The as-produced materials showed decomposition of W-ethoxide into WO_3 nano-particles suggesting that the photo-chemical process indeed occurred. Also worth describing here is the carrier gas system which is accomplished by a three-way nozzle having three concentric cylinders. The outer cylinder is connected to an argon supply. The argon guides the aerosol droplets which are carried by either C_2H_2 (supposedly non-reactive) or O_2 (highly reactive) gases interchangeably in the middle and second cylinder. This is illustrated in Fig. 1.

An aliquot of 5.4 mg of dark blue powder of WCl_6 (Aldrich 99.99%) was dissolved in 500 mL of ethanol. Since WCl_6 is highly reactive with air and moisture, its dissolution was conducted in an argon atmosphere. Particles from this process were collected on Corning glass substrates, placed on a rotating stage, at room temperature and at atmospheric pressure. The particle deposition showed a void at the centre (Fig. 1b) when the encapsulating carrier gas flow-rate was higher than the carrier gas driving the precursor droplets. When the flow-rates were reversed, the deposition showed the profile of a hump (Fig. 1a) showing there was more deposition at the centre

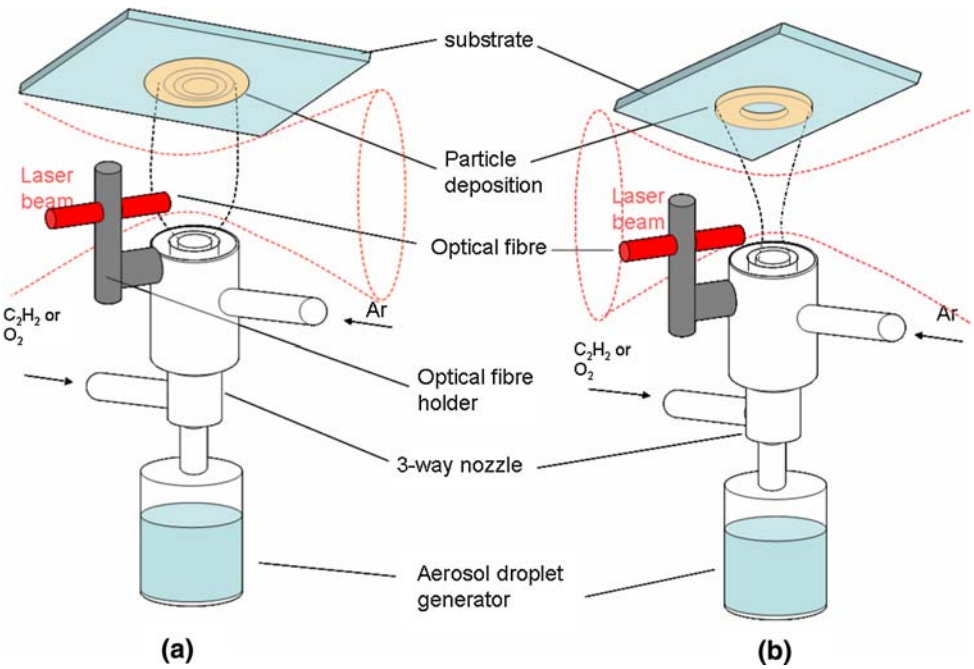

Fig. 1 Laser pyrolysis illustration and the role of carrier gas and precursor relative flow-rates (**a**) when the precursor flow-rate is larger than the encapsulating carrier gas (Ar) and (**b**) when the precursor flow-rate is smaller than the flow-rate of Ar. The precursor is driven either by C_2H_2 or O_2. The particle deposition in (**a**) has profile of a hump, whereas the deposition in (**b**) has a vacancy at the centre as indicated on the substrates

Table 1 The experiment parameter used to obtain the WO_3 samples by laser pyrolysis

Sample	Precursor	Gas 1 (8 cm^3/min)	Gas 2 (8 cm^3/min)	Gas 3 variable	Nano-wire yield	Morphology
W1	WCl_6 + Ethanol	O_2	Ar	Ar	High	Slabs + Rods
W2	WCl_6 + Ethanol	C_2H_2	Ar	Ar	Low	Sphere + Rod

of the substrate than in periphery. This was found to be in agreement with Bernoulli's theorem, which requires that there should be reduced pressure in fast flowing fluids. When the flow rate of the central gas is larger, the pressure is lower in this region and hence the droplets and the particles (after laser pyrolysis) are trapped in this low pressure region. Therefore there is high deposition at the centre of the substrate and vice versa. Table 1 lists the experimental procedures employed. The so-obtained samples were further annealed in argon atmosphere at 500 °C for 17 h. Morphology studies were carried out using a Jeol JSM-5600 scanning electron microscopy (SEM) microscope, which was also equipped for energy dispersive X-ray spectroscopy (EDX). In order to avoid charging effects during SEM analysis, the samples were made conductive by carbon/Au/Pd coating. Infrared and Raman spectroscopy experiments on the as-obtained WO_3 are reported elsewhere [17]. Structural studies were done using a Philips Xpert powder diffractometer equipped with a CuKα wavelength of 0.154184 nm. The experimental procedure showed good reproducibility of results.

Lengths and corresponding diameters of the nano-wires were measured by means of a software package ImageTool. As is the required procedure, calibration is initially made against the marker of known length in both the image scale and the real space scale. Then the distance between two points is measured for each point with accuracy that heavily depends on (1) the pixel density of the projecting screen, (2) the random errors from operator's hand and (3) the magnification of the image.

Results

Laser pyrolysis of tungsten-based precursors, with C_2H_2 as carrier gas, shows remarkable differences in morphology from when O_2 is the carrier gas as shown in Figs. 2 and 3. The C_2H_2-synthesized sample has a lower yield of WO_3 nano-wires after annealing than the O_2-synthesized one. These nano-wires in O_2-ran sample grow in the crevices of the film. The C_2H_2-ran sample has nano-wires with a higher aspect ratio than the O_2-ran samples. Also the C_2H_2-ran sample shows the presence of spherical micro-particles where as complete absence of these spheres is observed in the O_2-ran sample. This means that C_2H_2 maintains the spherical shape of the precursor droplets, which is clear evidence that C_2H_2 is only a sensitizer of the process but does not participate in the decomposition of the precursor. Also, in the presence of tungsten, C_2H_2 dissociates and forms carbon structures such as carbon nano-tubes. It was shown that vanadium surfaces can be used as catalysts for the growth of carbon nano-tubes [18] from C_2H_2. On the other hand, O_2 actively participates in the breakdown of the precursor droplets and in the process increases the yield of the WO_3 nano-wires at the expense of aspect ratio of the wires in general. The O_2-ran sample also has very brittle thin films with cracks in a somewhat ordered manner. This ordered cracking after annealing could be attributed to the growth pressure (thermal stress) from the 1D nanostructures.

The TEM micrograph of a typical wire grown from O_2-run WO_3 particles shown in Fig. 4b revealed a core-shell structure (redrawn in Fig. 4c) with the WO_x wire at the core (EDS in Fig. 4a) and the carbon–Au–Pd composite around the wire as a shell (EDS in Fig. 4e). C–Au–Pd is a material used in the prior-to-SEM coating to improve conduction for enhanced imaging. The shell is thicker on one side than on the other; that is, the wire is not centred through the C–Au–Pd wrapping. This shell served as a contamination, which obscured the electron diffraction of the wire so that the stoichiometry studies of the WO_x nanowire could not be accomplished. In line with our previous studies, we can speculate that the wire is WO_x with x being less than three due to oxygen loss during annealing even as elaborated in chemical reactions of the type in Eq. 4.

In order to observe the growth of nano-wires, we sonicated a few spheres of WO_3 into iso-propanol and placed them on carbon-holey Cu grid for in-situ annealing and imaging in a Jeol CM200 transmission electron microscope. A series of images, shown in Fig. 5, were taken periodically of intervals of 45 min whilst heating at temperatures ranging from 700 °C to 900 °C using a heating device specially tailored for this microscope. The images showed no indication of growth of one-dimensional structures. This is attributed to the vacuum typical of TEM. Any atoms that are sublimated from the spheres are immediately removed by the high vacuum giving a very small probability of condensing and growing into 1D nanostructured geometry. However, the shrinking of the spheres is an indication that the atoms are indeed evaporating from the surface. However, not all sublimated atoms are removed from their parent spheres; some return to make

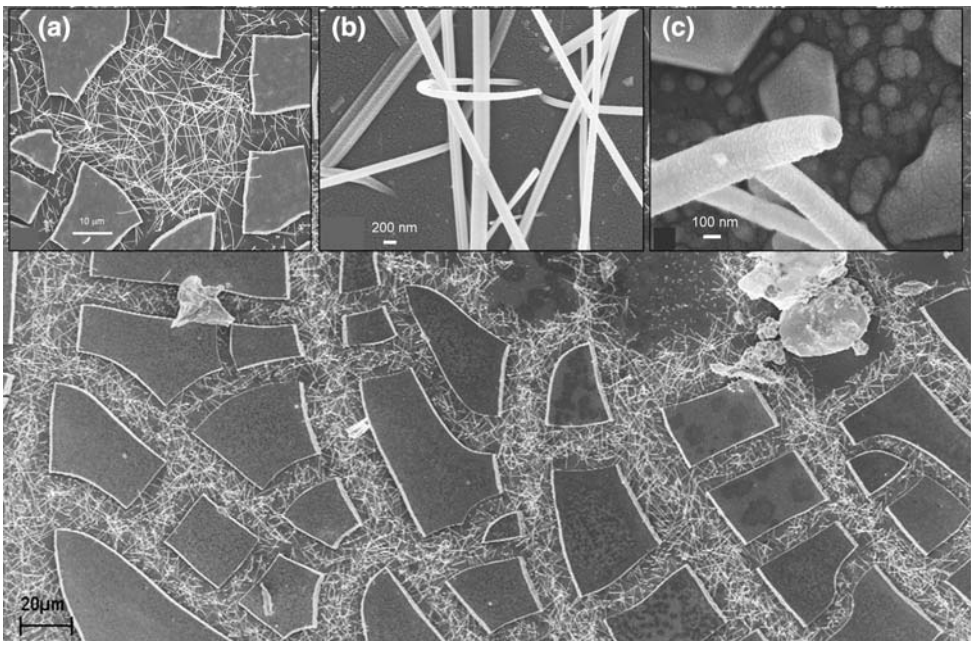

Fig. 2 Scanning electron micrographs of WO_3 nano-rods grown under oxygen as a central carrier gas and C_2H_2 as the secondary carrier gas showing a thin film that has flaked up into orderly slabs between which are numerous nano-wires. Inset (**a**) shows a close look at the nano-wires in between the slabs. Inset (**b**) zooms in onto the nano-wire area and inset (**c**) display one nano-wire's end

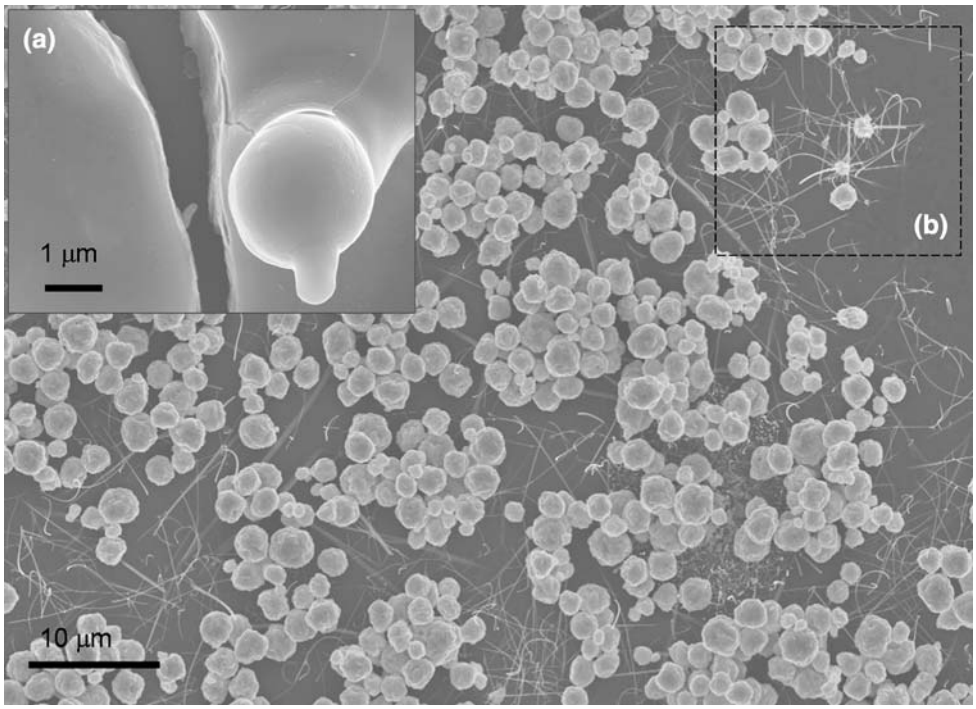

Fig. 3 Scanning electron micrographs of WO_3 nano-rods grown under C_2H_2 as a central carrier gas and oxygen as the secondary carrier gas. The spherical droplets from the precursor maintain their shape until their deposition into micro-particles. Inset (**a**) is a micro-particle before annealing showing the genesis of the growth of a nano-wire. After annealing there are numerous nano-wires growing from and in between the spheres. Dotted box (**b**) shows a region where a number of nano-wires are seen sprouting from spheres

small mounds on the sphere surface making the sphere rougher. The rate of sphere size reduction due to loss of atoms is depicted in Fig. 5b. It is interesting to note that the smaller sphere C shrank faster than the larger sphere B. This means that wires grown from small spheres grow faster than those that grow from large spheres.

For us to understand the novel growth of these nano-wires, it is important to briefly review some related growth mechanisms available in literature. Sir Frederick Frank proposed the 'screw dislocation theory' in 1949. Central to this dislocation theory were Polanyi, Orowan, Taylor, Burger and Mott & Nabarro [19]. Defects and dislocation in the initial crystals initiate one-dimensional growth; "…the crystal face always has exposed molecular terraces on which growth can continue, and the need for fresh 2D nucleation never arises…" [19]. In 1964, detailed studies on the morphology and growth of silicon whiskers by Wagner & Ellis [20] led to a new concept of crystal growth

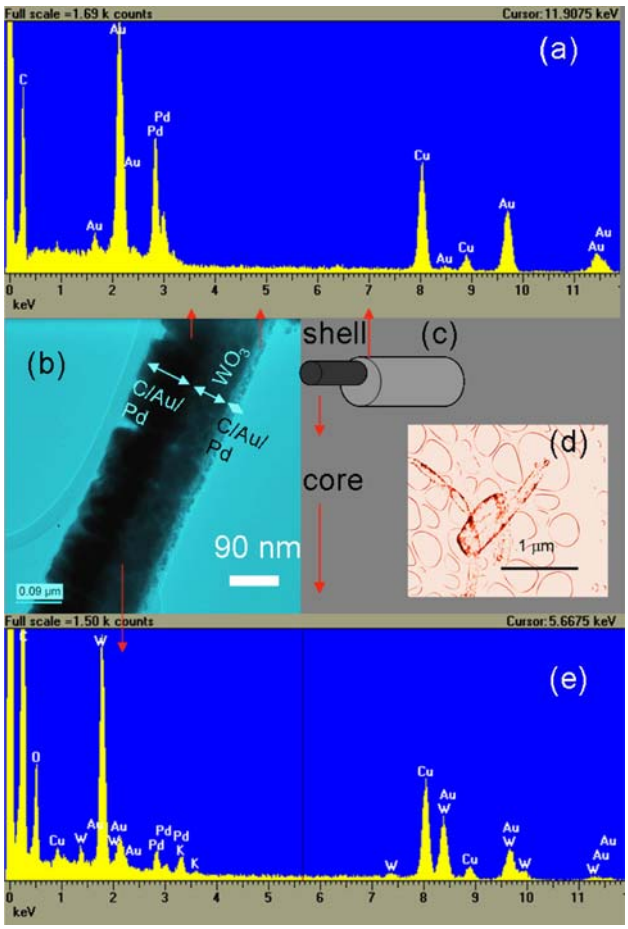

Fig. 4 TEM image of a WO_3 nano-wires in (**b**) reveals that the wire is a core with a shell of carbon, Au and Pd from prior-to-SEM coating as confirmed by EDS in (**a**) and (**e**). Inset (**c**) is an illustration of the core-shell structure of the WO_3 nano-wire and C/Au/Pd layer and (**d**) is TEM image of carbon nanotubes found alongside the WO_3 nano-wires

from vapour, which was called the vapour–liquid–solid (VLS) mechanism. The new growth mechanism was built around three important facts: (a) silicon whiskers did not contain an axial screw dislocation (b) an impurity was essential for whisker growth and (c) a small globule was always present at the tip of the whisker during growth. From fact (a), it was clear that growth from vapour did not occur according to Frank's screw dislocation theory and from, facts (b) and (c), it was important that a new growth mechanism be studied.

In 1975, Givarzigozov [21] introduced the fundamental aspects of the VLS mechanism. Emphasis was placed on the dependence of the growth rate on the whisker diameter. It was found that the growth rate decreased abruptly for submicron diameters and vanished at some critical diameter $d_c \leq 0.1$ μm in accordance with the Gibbs–Thomson effect. Basing on this effect, which states that the solubility limit of a precipitate (β) in a matrix (α) varies with the precipitate's radius, Givarzigozov suggested that the effective difference between the chemical potential of the precipitate in the vapour phase and in the terminal precipitate [whisker], $\Delta\mu$, is given by

$$\Delta\mu = \Delta\mu_0 - \frac{4\Lambda\sigma}{D} \tag{1}$$

$\Delta\mu_0$ is the difference at a plane boundary (when diameter, D, of the precipitate tends to ∞), Λ is the atomic volume of the precipitate and σ is the surface free energy of the precipitate. The dependence of growth rate, G, on the super-saturation ($\Delta\mu/k_BT$) given by $V = b(\Delta\mu/k_BT)^n$, where b and n are coefficients to be evaluated from experimental data, was used to derive an expression

$$V^{1/n} = \frac{\Delta\mu_0}{k_BT} b^{1/n} - \frac{4\Lambda\sigma}{k_BT} b^{1/n} \frac{1}{D} \tag{2}$$

The main characteristics of VLS mechanism are (1) the presence of a catalyst and (2) direct proportionality of the diameter of the nanostructure to the growth rate. Thick whiskers grow longer than thinner ones because this growth can be afforded by the continual supply of building blocks in the CVD system. Plotting the growth rate, V, [21] or terminal length l_∞ [22] of the whisker versus D gives curves with a positive ascent. A plot of $V^{1/n}$ versus $1/D$ gives a straight line graph with a negative slope [21].

Recently, an in situ growth profile in real time for tungsten oxide nano-wires was followed by Kasuya et al. (2008) [23] by injecting ultra-small flow-rates of O_2 on a heated tungsten surface placed on a scanning electron microscope stage. It was difficult to ascertain if the length-and-diameter data would be in agreement with the VLS mechanism because the images were rather poor. This was due to the poor vacuum caused by the intentional injection of O_2, which was useful for the targeted reaction. The length of the nano-wire as a function time $l(t)$ was found to take the form of

$$l(t) = l_0[1 - \exp(-\alpha t)] \tag{3}$$

where l_0 is the final length and α is the growth or decay coefficient.

We however study the final state of the fully grown WO_3 nanostructures. Our present length-diameter data for the nano-wires could not agree with the above VLS theory for two conflicting reasons: (1) no particular catalyst could be identified with certainty (2) we found an inverse proportionality between length and diameter of the nano-wires. It was therefore important to study a new model to attempt to explain the new findings. Since the production of solid-state nano-wires is after annealing of the solid-state particles, the mechanism of growth can neither be according to liquid-based "Solution-Liquid-Solid" mechanism proposed by Trenter and Buhro [24, 25] nor in line with the "Super-Critical Fluid Synthesis" mechanism proposed by Holmes

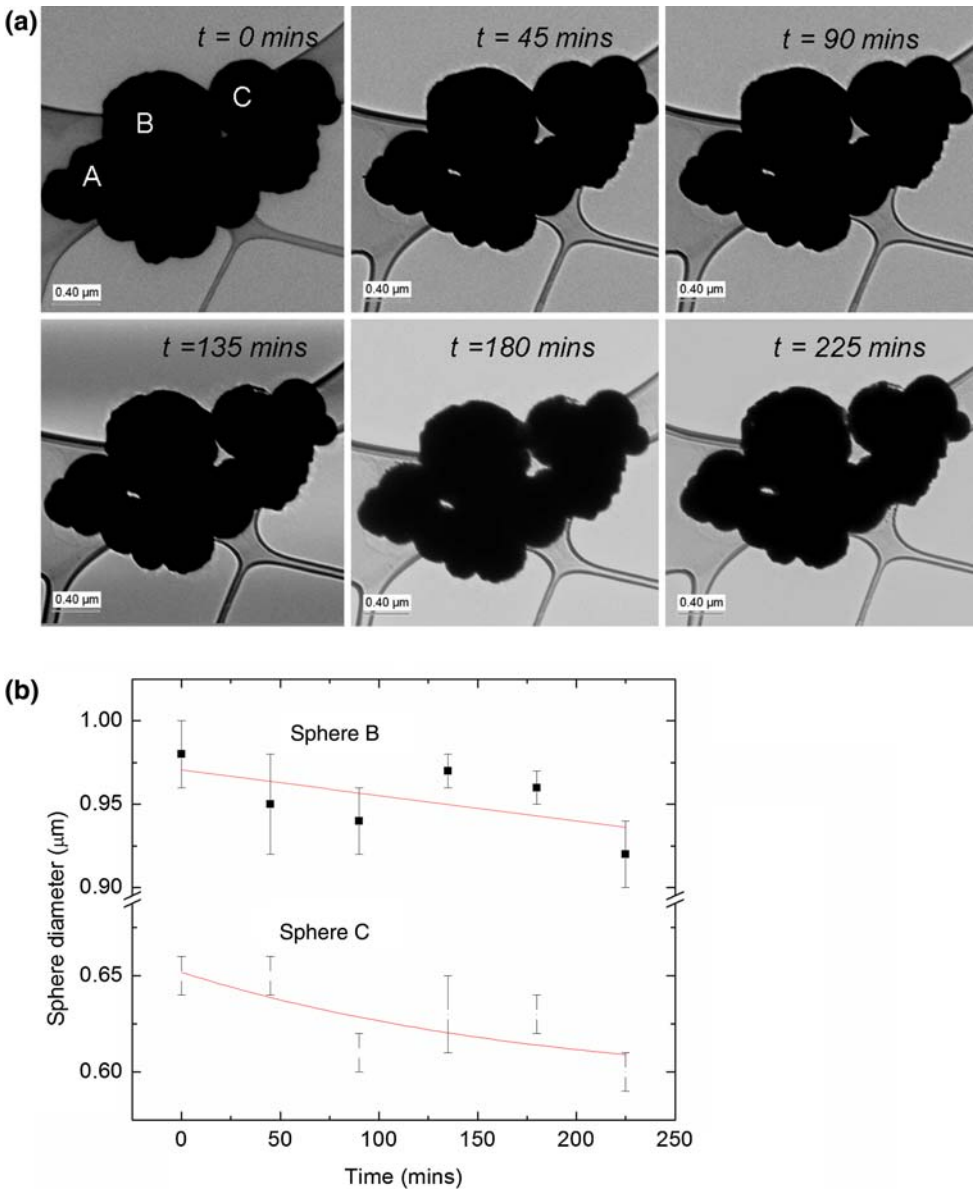

Fig. 5 In situ TEM annealing of WO_3 micro-spheres in vacuum at 700–900 °C. Micrographs were taken periodically as shown in (**a**). Note the variation of spheres A, B and C and the enlargement of space around these spheres as time of annealing increases. The variation of sphere diameter with time for sphere B and C are plotted in (**b**). Exponential decay curves are fitted and show that the smaller sphere C shrinks faster than B

[26] and which has been later supported by Korgel and co-workers [27]. These data certainly support our newly proposed "Solid–Vapour–Solid (SVS)" mechanism reported in our previous publication [28] where we reported solid-state $W_{18}O_{49}$ nano-tips produced by annealing solid-state WO_3 nano-spheres (prepared by ultrasonic spray pyrolysis) in argon environment. Synthesis of solid materials from solid precursors is not new. Solid-state reactions are very slow and difficult to carry out to completion unless carried out at very high temperatures where reacting atoms can diffuse through solid material to the reaction front more easily. Transformation of one phase to another (with the same chemical composition) can also occur in solid state, either at elevated temperatures or elevated pressures (or both). For the growth rate of many solid-state reactions (including tarnishing), inter-diffusion of ions through the product layer increases the thickness Δx parabolically with time $(\Delta x)^2 \propto t$ [29]. This is a sharply different dependence from the Eq. 1 proposed by Kasuya et al. [23] above. In some solid-state processes, nucleation can be homogeneous. This is often the case for thermal decomposition, for example, as is the case in the current reactions

$$\mathrm{WO_3}\begin{pmatrix}\text{spheres}/\\ \text{slabs}\end{pmatrix} \xrightarrow{500\,^{\circ}\mathrm{C};\quad 17\,\mathrm{h};\quad \text{Argon}} \mathrm{WO}_x(\text{nanowires}) + \mathrm{O_2} \qquad (4)$$

In this Letter, we introduce for the first time the statistical-mechanical aspects of this proposed SVS model and fit the ensuing mathematical expressions to the data.

For the sake of simplicity, we consider the source of molecules to be a solid sphere of radius R_0, containing

molecules of mass, M and assume the molecules to be spherical of average molecular diameter, Ω. We assume further that in changing the morphology from a sphere to a wire, only the surface molecules can migrate from the sphere to the newly forming wire or rod. For instance it has been demonstrated [30] that the surface diffusive flux, J_S of atoms on a surface of a slab of length L given by $J_S = -(\mathrm{d}c/\mathrm{d}x)\int_0^L D(y)\mathrm{d}y$ is different from the more familiar bulk diffusive flux written from the first Fick's law as $J_B = -D_B(\mathrm{d}c/\mathrm{d}x)L$ where $\mathrm{d}c/\mathrm{d}x$ is the concentration gradient. In this case, transformation from sphere to rod takes place layer after layer. The sphere shrinks but the as-forming rod lengthens as illustrated in Fig. 6.

If the sphere is amorphous and the wire is crystalline as normally observed experimentally, then the densities of the material in the initial sphere and the final wire are different and can be written, respectively, as ρ_{am} and ρ_{cryst}. The number of atoms in the first layer of the sphere can therefore be written as

$$N_1^{surf} = 4\pi R_0^2 \Omega \frac{\rho_{am}}{M} \tag{5}$$

If all these atoms assemble into a rod of diameter D and length l_1 then the number of molecules in the rod can be written in terms of length l_1 as

$$N_1^{rod} = \frac{\pi}{4} D^2 l_1 \frac{\rho_{cryst}}{M} \tag{6}$$

However, not all the atoms in Eq. 5 end up making the rod. The actual fraction that self-assembles into the rod is proportional to the Boltzmann's fraction, which depends on the temperature T of the ambient given as

$$\frac{N_1^{rod}}{N_1^{surf}} = \exp\left(-\frac{E_A}{k_B T}\right) \tag{7}$$

E_A is the activation energy of the atoms.

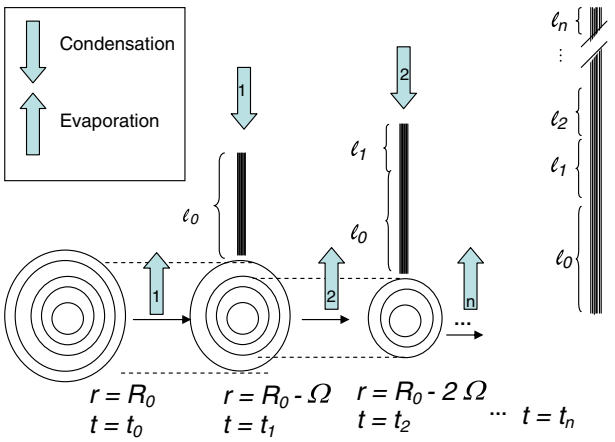

Fig. 6 Proposed schematic of the solid–vapour–solid mechanism of growth of 1D nano-structure from a spherical layer of atoms in a tip growth

After the first layer has assembled into the rod of length l_1, the next layer in the sphere has a radius of $R_0-\Omega$ which forms the next segment of the rod of length l_2. The subsequent layers have radii of $R_0 - 2\Omega$, $R_0 - 3\Omega$, $R_0 - 4\Omega$, $R_0 - 5\Omega$ and so forth. The ith layer will have a radius of $R_0-(i-1)\Omega$ such that the number of atoms in the ith layer is

$$N_i^{surf} = 4\pi\Omega \frac{\rho_{am}}{M}[R_0 - (i-1)\Omega]^2 \tag{8}$$

This corresponds to the number of atoms in the ith segment of the rod of length l_i given as

$$l_i = 16\frac{\rho_{am}\Omega}{\rho_{cryst}}\exp\left(-\frac{E_A}{k_B T}\right)[R_0 - (i-1)\Omega]^2\frac{1}{D^2} \tag{9}$$

The total length of the wire is a summation of all the segments of the wire emanating from each corresponding layer in the source sphere.

$$l = l_1 + l_2 + l_3 + \ldots + l_N = \sum_i^N l_i = \zeta\frac{1}{D^2} \tag{10}$$

where

$$\zeta = 16\frac{\rho_{am}\Omega}{\rho_{cryst}}\exp\left(-\frac{E_A}{k_B T}\right)\sum_i^N [R_0 - (i-1)\Omega]^2 \tag{11}$$

Parameter ζ is a function of temperature T and also depends on the geometry of the source of the atoms. The higher the annealing temperature, T, the higher the slope, ζ. This fact may mean that thinner nano-wires can be obtained at higher annealing temperatures. But there must be a lower limit to how thinner the nano-wires can get in the SVS mechanism since at much higher temperatures all solid-state starting material should evaporate away leaving nothing to form the nano-wires with. These limits are yet to be determined. The same question has been asked if there is a thermo-dynamical lower limit to the nano-wires growth by VLS [31]. It can be seen that if the source is equally crystalline then the ratio of the densities in the source to the final structure is unity. By quick inspection, one can see that the geometry described by the summation in Eq. 11 is proportional to the total surface area of all atomic or molecular layers in the source. A plot of l versus $1/D^2$ should be a positive straight line graph with a y-intercept of zero and a slope of ζ. Similarly a plot of aspect ratios l/D versus $1/D^3$ is supposed to be a positive straight line going through the origin and having the slope, ζ.

In the VLS mechanism, given a constant flux of molecules in the source, a nano-wire that has a large diameter will grow much longer compared to when it starts out with a small diameter. In the SVS growth, the thinner the wire the longer it is and vice versa as shown in the plots of Fig. 7a. When aspect ratios, defined here as the ratio of length to diameter, is plotted against diameter, the same

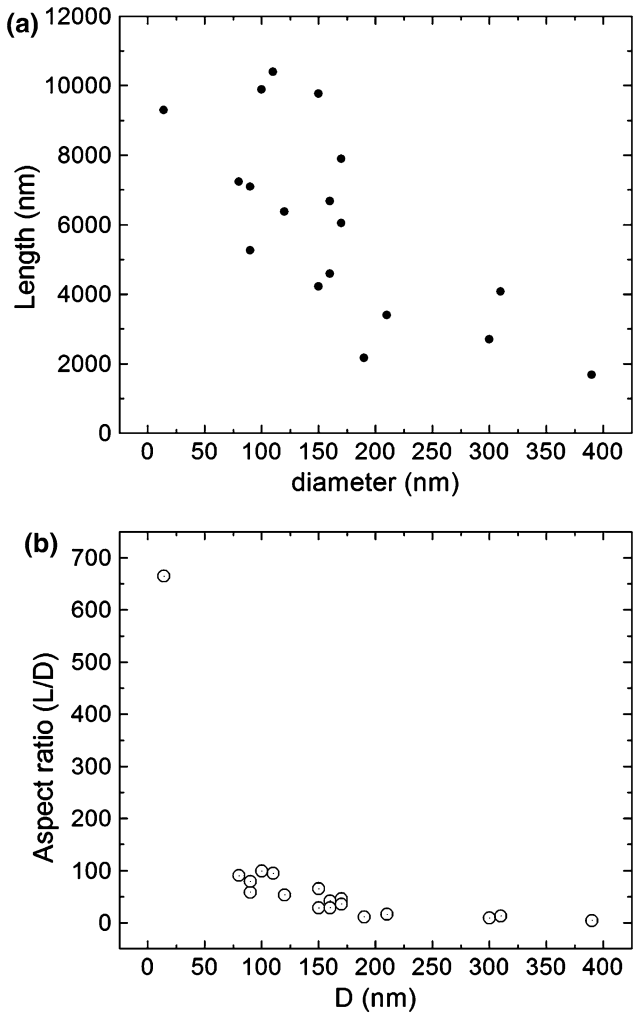

Fig. 7 Scatter plots of (**a**) length of the nano-wire versus the corresponding diameter (**b**) aspect ratio versus diameter

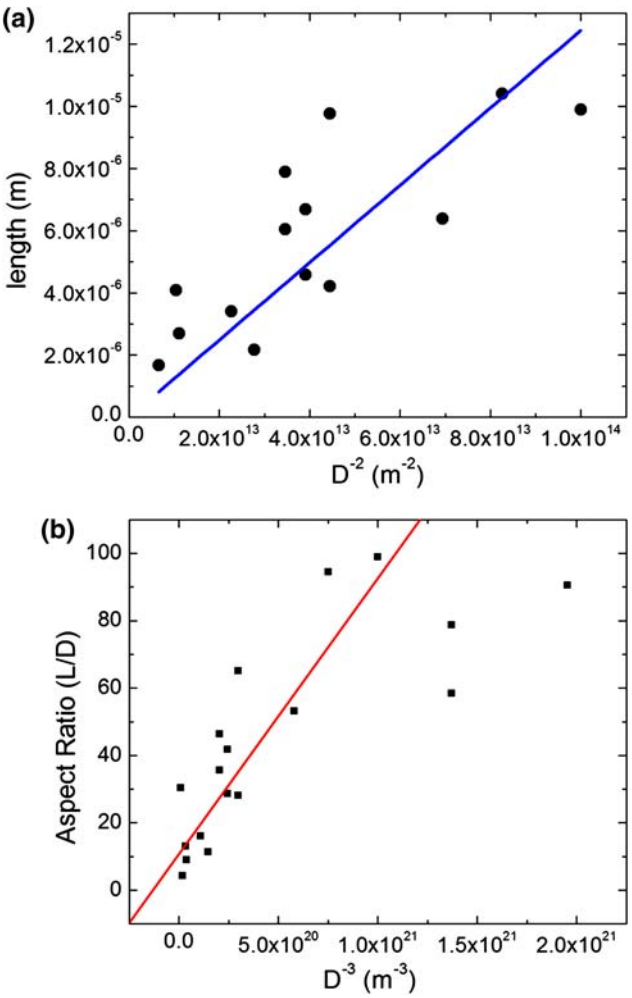

Fig. 8 Scatter plots of (**a**) length versus $1/D^2$ and (**b**) aspect ratio (L/D) versus $1/D^3$. The linearized plots (**a**) and (**b**) have similar slopes within experimental error as predicted by the current theory [$(6.22 \pm 2.77) \times 10^{-20}\ m^3$ and $(6.25 \pm 0.831) \times 10^{-20}\ m^3$, respectively]

profile is obtained (Fig. 7b). When length and aspect ratio are plotted against $1/D^2$ and $1/D^3$, respectively, in accordance with Eq. 10, positive slopes are manifested (Fig. 8) almost equal to each other as expected from the above theory and of the order of $\sim 10^{-20}\ m^3$. This value is related to the order of magnitude of the average volume of the WO_3 nano-wires. It should be noted that reverse growth from one-dimensional to spherical particles is also possible at suitable annealing conditions. For instance, nano-belts of Zn acetate were converted into aggregates of ZnO nano-particles as reported in this journal [32].

Conclusion

In summary, liquid atomization and subsequent laser pyrolysis were carried out using a CO_2 laser tuned at its $10P_{20}$ line of wavelength 10.6 μm. SEM characterization of the as-produced WO_3 samples showed that selective photochemical reactions by the laser have a part to play in initiating self assembly growth centres even without the need for a catalyst. Self assembly is only continued by further annealing. We have shown that oxygen carrier gas gives a higher yield of WO_3 nano-wires by laser pyrolysis than acetylene. The latter also shows trace amounts of multi-walled carbon nano-tubes. The transmission electron microscopy reveals that the nano-wires are core-shell structures of a mixture of Au, Pd and C in the shell and WO_3 at the core. The shell is due to the prior-to-SEM coating to improve imaging. The absence of catalysts in addition to the analysis of the nano-wire length-and-diameter data has validated a new growth mechanism, which we have called SVS growth as proposed earlier [28].

Acknowledgements Authors would like to thank Prof. Michael Witcomb, Mr. Mthokozisi Masuku, Mr. Henk van Wyk and Ms. Retha Rossouw. The South African Department of Science and

Technology (DST) project for the African Laser Centre, the National Research Foundation (NRF), the DST/NRF Centre for Excellence in Strong Materials and the CSIR National Centre for Nano-Structured Materials are acknowledged.

References

1. P.A. Cox, *Transition Metal Oxides: An Introduction to Their Electronic Structure and Properties* (Oxford University Press, Oxford, 1992)
2. C.G. Granqvist, A. Azens, A. Hjelm, L. Kullman, G.A. Niklasson, D. Rönnow et al., Sol. Energy **63**, 199 (1998). doi:10.1016/S0038-092X(98)00074-7
3. C.G. Granqvist, E. Avendano, A. Azens, Thin Solid Films **442**, 201 (2003). doi:10.1016/S0040-6090(03)00983-0
4. A. Hoel, L.F. Reyes, P. Heszler, V. Lantto, C.G. Granqvist, Curr. Appl. Phys. **4**, 547 (2004). doi:10.1016/j.cap.2004.01.016
5. M. Bendahan, R. Boulmani, J.L. Seguin, K. Aguir, Sens. Actuators **100**, 320 (2004). doi:10.1016/j.snb.2004.01.023
6. R.F. Mo, G.Q. Jin, X.Y. Guo, Mater. Lett. doi:10.1016/j.matlet.2006.12.061
7. Y. Shigaya, T. Nakayama, M. Aono, Sci. Technol. Adv. Mater. **5**, 647 (2004). doi:10.1016/j.stam.2004.02.021
8. M. Gillet, K. Aguir, M. Bendahan, P. Mennini, Thin Solid Films **484**, 358 (2005). doi:10.1016/j.tsf.2005.02.035
9. C. Bittencourt, R. Landes, E. Llobert, G. Molas, X. Correig, M.A.P. Silva et al., J. Electrochem. Soc. **149**, H81 (2002). doi:10.1149/1.1448821
10. P. Ivanov, J. Hubalek, K. Malysz, J. Prasek, X. Vilanova, E. Llobert et al., Sens. Actuators B **100**, 293 (2004). doi:10.1016/j.snb.2003.12.065
11. C.L. Dai, M.C. Liu, F.S. Chen, C.C. Wu, M.W. Chang, Sens. Actuators B Chem. (2006). doi:10.1016/j.snb.2006.10.055
12. J. Rajeswari, P.S. Kishore, B. Viswanathan, T.K. Varadarajan, Nanoscale Res. Lett. **2**, 496 (2007). doi:10.1007/s11671-007-9088-y
13. X.P. Wang, B.Q. Yang, H.X. Zhang, P.X. Feng, Nanoscale Res. Lett. **2**, 405 (2007)
14. H.R. Bachmann, H. Noth, R. Rinck, K.S. Kompa, Chem. Phys. Lett. **29**, 627 (1974). doi:10.1016/0009-2614(74)85107-9
15. C.M. Bowden, J.D. Stettler, N.M. Witriol, J. Phys. B Atom. Mol. Phys. **10**, 1789 (1977). doi:10.1088/0022-3700/10/9/028
16. B.W. Mwakikunga, A. Forbes, E. Sideras-Haddad, R.M. Erasmus, G. Katumba, B. Masina, Int. J. Laser Nanoparticles (2008) (in press)
17. B.W. Mwakikunga, E. Sideras-Haddad, A. Forbes, C. Arendse, Phys. Status Solidi **205**, 150 (2008). doi:10.1002/pssa.200776829
18. J.W. Seo, K. Hernadi, C. Miko, L. Forro, Appl. Catal. Gen. **260**, 87 (2004). doi:10.1016/j.apcata.2003.10.003
19. F.C. Frank, Discuss Faraday Soc. **5**, 48 (1949). doi:10.1039/df9490500048
20. R.S. Wagner, W.S. Ellis, Appl. Phys. Lett. **4**, 89 (1964). doi:10.1063/1.1753975
21. E.I. Givargizov, J. Cryst. Growth **31**, 20 (1975). doi:10.1016/0022-0248(75)90105-0
22. J. Kikkawa, Y. Ohno, S. Takeda, Appl. Phys. Lett. **86**, 123109-1 (2005). doi:10.1063/1.1888034
23. K. Kasuya, T. Ooi, Y. Kojima, M. Nakao, Appl. Phys. Express **1**, 034005 (2008). doi:10.1143/APEX.1.034005
24. T.J. Trenter et al., Science **270**, 1791 (1995). doi:10.1126/science.270.5243.1791
25. W. Buhro, Adv. Mater. Opt. Electron. **6**, 175 (1996). doi:10.1002/(SICI)1099-0712(199607)6:4<175::AID-AMO236>3.0.CO;2-C
26. J.D. Holmes et al., Chem. Eur. J. **9**, 2144 (2003). doi:10.1002/chem.200204521
27. T. Hanrath, B. Korgel, Adv. Mater. **5**, 15 (2003)
28. B·W. Mwakikunga, E. Sideras-Haddad, C. Arendse, M.J. Witcomb, A. Forbes, J. Nanosci. Nanotechnol. (2008) (in press)
29. S. Elliot, *The Physics of Chemistry of Solids* (Wiley, Chichester, 2000)
30. J.B. Hudson, *Surface Science—An Introduction* (Butterworth-Heinemann, Boston, 1992)
31. T.Y. Tan, N. Li, U. Gosele, Appl. Phys. Lett. **83**, 1199 (2003). doi:10.1063/1.1599984
32. Y. Zhang, F. Zhu, J. Zhang, L. Xia, Nanoscale Res. Lett. **3**, 201 (2008). doi:10.1007/s11671-008-9136-2